Autocorrelation and Regularization in Digital Images I. Basic Theory

DAVID L. B. JUPP, ALAN H. STRAHLER, MEMBER, IEEE, AND CURTIS E. WOODCOCK

Abstract—**Spatial structure occurs in remotely sensed images when the imaged scenes contain discrete objects that are identifiable in that their spectral properties are more homogeneous within than between them and other scene elements. The spatial structure introduced is manifest in statistical measures such as the autocovariance function and variogram associated with the scene, and it is possible to formulate these measures explicitly for scenes composed of simple objects of regular shapes. Digital images result from sensing scenes by an instrument with an associated point spread function (PSF). Since there is averaging over the PSF, the effect induced in the image data by the instrument (called regularization here) will influence the observable autocovariance and variogram functions of the image data. This paper, the first of two, shows how the autocovariance or variogram of an image is a composition of the underlying scene covariance convolved with an overlap function, which is itself a convolution of the PSF. The functional form of this relationship provides an analytic basis for scene inference and eventual inversion of scene model parameters from image data.**

Keywords—**Remote sensing, digital image, spatial statistics, autocovariance, regionalized variable, variogram.**

I. INTRODUCTION

OVER THE past six years, the authors, separately and together, have carried out a number of studies in remote sensing that have utilized interpixel variance to analyze and model digital images. Three major lines of research have been pursued. In chronological order, the first was the development of geometric-optical models of conifer forest canopies that were invertible using the variance of brightness values within the pixels drawn from a uniform conifer stand [1], [2]. This line continues today in the further refinement of the approach and its extension to other types of canopies. Second was the examination of spatial structure in remotely sensed images of real scenes, including spatial covariance functions, variograms, and examination of the behavior of interpixel variance as images are collapsed into ever-larger pixels through averaging [3]–[6]. Third was the development of three-dimensional models of self-shadowing within multilayer canopies and their application to modeling Landsat signatures of vegetation cover types as a function of vegetation geometry and sun angle [7], [8]. As this work emerged, two key concepts were developed as a guiding schema: the discrete-object model of the scene [9], and a taxonomy of scene models according to the size of the objects and the size of the resolution cell of the sensor [10].

Throughout this work, it became obvious that a coherent mathematical foundation existed that was being drawn upon directly or indirectly, sometimes with differing emphasis or perspective, and which provided a framework and context for the differing lines of enquiry. This paper, which is divided into two parts, attempts to provide that foundation. Part I, presented here, develops the basic theory in the context of remote sensing. Part II explores the application of the theory to some simple models of scenes and the digital images obtained from them.

A. Remote Sensing Context

In many applications of remote sensing and digital image processing, it is reasonable to regard a scene as a spatial arrangement of two- or three-dimensional objects superimposed upon a background. In such a case, we can consider a discrete-object scene model as an appropriate abstraction of the scene [9]. In this type of model, the scene includes one or more classes of objects, each of which has a set of unique properties or parameters that characterize it. As an example, an agricultural region in the midwestern U.S. could be regarded as a two-dimensional patchwork of rectangular objects (fields) of perhaps one to three different basic sizes. The reflectance of each field is determined by the state of the soil and crop within it. A conifer forest presents a three-dimensional example. Here, a forest scene might be modeled as a collection of green cones of a constant shape but varying size that are scattered randomly on a snow-covered plane and cast shadows on the snowy background as well as on other cones [1], [2].

The spatial structure of real scenes induces a measurable spatial structure in the images derived from them. This occurs since distinguishable objects tend to be spectrally homogeneous and separable from other objects and background. Adjacent points in the scene are consequently more similar spectrally than might be expected on average and the mean distance at which this "spatial autocorrelation" disappears is related to the size, spacing,

Manuscript received June 22, 1987; revised March 2, 1988. This work was supported by NASA under grants NAG 5-273, NAG 5-276, NAS 9-16664, (subcontract L200080), and NAGW-735.

D. L. B. Jupp is with the Division of Water Resources Research, Commonwealth Scientific and Industrial Organization, P.O. Box 1666, Canberra, ACT, 2061, Australia.

A. H. Strahler is with the Department of Geology and Geography, Hunter College of the City University of New York, New York, NY 10021.

C. E. Woodcock is with the Department of Geography and Center for Remote Sensing, Boston University, Boston, MA 02215.

IEEE Log Number 8821445.

and shape of the objects in the scene. The induced spatial structure will also depend greatly on the spatial resolution of the sensor as compared to the objects that are being imaged. If the resolution cells are small with respect to the objects, then it will be possible to identify the size and shape of each object as well as to examine the brightness values within it. We refer to this situation as the *H*-resolution case [10]. As an example, consider a Landsat MSS (multispectral scanner) image of the agricultural scene described above. In the Landsat MSS system, each pixel (picture element) is associated with a resolution cell of 79-m width in the scene. When fields are many times larger than the resolution cell size, the image of each field will contain many pixels. Therefore, adjacent pixels will tend to fall within the same field, and hence be spatially autocorrelated.

In contrast is the *L*-resolution case, in which the resolution cell is larger than the objects within the scene. In the *L*-resolution image, each digital value represents a brightness for a combination of objects and background. A Landsat image of the conifer forest scene provides an example of an *L*-resolution model. Since the tree crowns will be considerably smaller than the sensor's resolution-cell size, each pixel will include a number of objects (trees). If the forest is relatively dense, adjacent brightness values will be strongly correlated since the number of trees within each resolution cell will remain more or less uniform from one resolution cell to the next. However, if the forest is quite sparse, there may be considerable chance variation in the number of trees within each resolution cell and thus adjacent-pixel correlation will be reduced.

Clearly this situation will change as the spatial resolution of the sensor system changes. At the 20- or 10-m resolution of the French SPOT satellite system, there will be a strong interaction in the forest scene between the size of the resolution cell and the size of the trees. At this resolution, even a fairly dense, uniform forest will vary considerably from pixel to pixel in a digital image. With a large resolution cell size, such as the 1.1-km resolution of NOAA's advanced very high resolution radiometer (AVHRR) instrument, averaging will be sufficiently great that there will be little or no spatial variation in pixel brightness even within a sparse woodland.

These simple considerations show how the spatial structure and statistics of digital images will be greatly influenced by 1) the size, shape, and density of objects in the scene, and 2) the relationship between the size of the objects and the size of the resolution cells in the digital image of the scene.

The study of spatial structure in images can be approached from two directions. First, it is possible to define various parameters that measure spatial structure and calculate them for real images [3]. With an understanding of such measurements and how they interact with various types of scenes as imaged at different resolutions, it is possible to gain considerable insight into the influence of spatial structure on the information extraction process [4]. Second, it is possible to adopt a scene-modeling approach, beginning with simple scenes of discrete elements and deriving their intrinsic spatial structures and the spatial structures they induce in images taken from them. This paper, the first in a series, approaches the problem from the second perspective. It provides a proper mathematical framework for consideration of digital images, and derives results that can be used to describe 1) the autocorrelation structure of images composed of discrete objects, and 2) how that structure is influenced by regularization—a process of spatial averaging that arises when a sensor makes a measurement that is integrated over a finite area of the scene. Further articles will move to models and simulations of simple, theoretical scenes, and then examine the spatial structure of real images.

II. Theory of Spatial Covariance

A. Regionalized Variables

Consider the scanning and imaging of a scene by a remote-sensing device. The output of the scanner will be a set of measurements, each of which is associated with a spatial position. In mathematical terms, these measurements can be considered as values of a "regionalized variable"—brightness as a function of spatial position. An extensive body of theory devoted to the study of spatial pattern and variation in regionalized variables now exists. It has been developed through various applications, including those of geostatistics, which is the estimation of geological parameters from spatial samples; stereology, the study of projections and sections of multidimensional objects into spaces of lower dimension and image analysis, or the study of shapes and structures in two-dimensional images.

This paper borrows much from the theory of regionalized variables [11], especially as developed by Matheron [12]–[14] and Serra [15]. In this sense, our treatment is not new—these authors have gone over the same ground, albeit in a much more abstract fashion. However, our treatment has been developed with specific reference to digital imaging of objects on the earth's surface. As such, it presents a concrete foundation for a proper mathematical description of the spatial structure of digital images and the inference of scene structure from image data.

B. Stochastic Nature of the Scene

For application of a mathematical theory, we will adopt a stochastic view of the landscape and its spatial structure. In this approach, we assume that there are underlying properties and processes of the landscape that produce many similar scenes. For example, consider an agricultural area in which the given topography, soils, climate, and sociocultural factors influence the sizes and shapes of fields and the crops they contain. An individual scene drawn from such a region will be unique, but will also be similar to all other such scenes in many respects.

Mathematically, this can be stated more formally as applied to digital images. Consider a spatial random func-

tion f that generates radiance values $f(x)$ as a function of spatial position x. (Here x is regarded as a vector variable—which is in this case a pair of image coordinates.) A digital image, which expresses radiance as a function of spatial position, may be regarded as a single realization of such a function—and, for the purpose of analysis, as a regionalized variable [16], [17].

Consider now summary statistics (such as the mean, observed spatial covariance, etc.) that are derived from a digital image. We can adopt the deterministic view that these are unique and intrinsic to the image only, or we may adopt a stochastic view that such statistics also characterize the properties of the underlying spatial function. Obviously, if we want to infer something about the spatial properties and processes of the landscape, we will of necessity assume the latter view. Mathematically, two assumptions are required: spatial stationarity, which assumes that the parameters of the underlying function do not vary with spatial position; and ergodicity, which assumes that spatial statistics taken over the area of the images as a whole are unbiased estimates of those parameters. These assumptions will be introduced at appropriate points in the following exposition.

C. Covariance for Random Functions

The question arises as to what statistics are sufficient to characterize the spatial random function, particularly when only an image of a single realization of it is available. When the underlying scene is an image model, we also wish to establish what statistics are sufficient to characterize the parameters of the model. In the following work in this and later papers, we have made extensive use of second-order spatial statistics, such as the spatial covariance and variogram. The effectiveness of this statistic for estimating parameters of image models will be established in later papers. Here, we examine its basic properties.

Since covariance describes the behavior of the function at one point relative to its behavior at another point, it can also be regarded as an autocovariance. The (auto)covariance between two values at points x_1 and x_2 in N-dimensional space ($\boldsymbol{R}^N$) induced by the random function $f(x)$ is

$$\mathrm{Cov}_f(x_1, x_2) = E\Big\{\big[f(x_1) - m(x_1)\big] \cdot \big[f(x_2) - m(x_2)\big]\Big\}. \quad (1)$$

In this expression, $m(x) = E\{f(x)\}$ is the mean of the process at x, $E\{\ \}$ denotes the expectation, and the expectations are taken as averages over the ensemble of realizations of f at the fixed points x_1 and x_2.

Introducing a second random function $g(x)$, the cross-covariance between points x_1 and x_2 induced by random functions f at x_1 and g at x_2 is similarly defined as

$$\mathrm{Cov}_{f,g}(x_1, x_2) = E\Big\{\big[f(x_1) - m_f(x_1)\big] \cdot \big[g(x_2) - m_g(x_2)\big]\Big\}. \quad (2)$$

This statistic, which is not symmetric in x_1 and x_2, is important in multichannel images where image spatial analysis considers the full spatial covariance matrix to characterize the underlying processes. For simplicity, however, this paper will be concerned almost entirely with single functions.

Consider the case in which $m(x)$ is independent of x (i.e., is stationary throughout $\boldsymbol{R}^N$) and $\mathrm{Cov}_f(x_1, x_2)$ depends only on the relative position h of the two points, i.e., $h = (x_1, x_2)$. We shall denote this type of covariance as

$$\mathrm{Cov}_f(h) = E\Big\{\big[f(x) - m\big]\big[f(x+h) - m\big]\Big\}. \quad (3)$$

In this case, f is "wide-sense" stationary. In geostatistics, a more relaxed form of stationarity is usually assumed and, rather than the covariance function, the related variogram function is used to characterize spatial structure

$$V_f(h) = E\Big\{\big[f(x) - f(x+h)\big]^2\Big\}. \quad (4)$$

The variogram simply describes the average squared difference between values as a function of the distance between them. For the two-function case, the cross-variogram is similarly defined as

$$V_{f,g}(h) = E\Big\{\big[f(x) - f(x+h)\big]\big[g(x) - g(x+h)\big]\Big\}. \quad (5)$$

These functions are closely related to the covariance. If the variance of the random function is finite (i.e., the function has a mean and is wide-sense stationary), some simple manipulation shows that

$$V_f(h) = 2\big[\mathrm{Cov}_f(0) - \mathrm{Cov}_f(h)\big] \quad (6)$$

$$V_{f,g}(h) = 2\big[\mathrm{Cov}_{f,g}(0) - \mathrm{Cov}_{f,g}(h)\big]. \quad (7)$$

If the variogram is used, the assumption that $m(x)$ (the "trend" of the spatial function) does not vary may be relaxed. All we need assume is that $m(x)$ does not change significantly within the range h. In this case the regionalized variable is said to be "stationary in increments." The stationarity of the variogram, however, is a fundamental assumption in geostatistics and is usually appropriate in digital image processing. This is because images, although not wide-sense stationary due to scan angle effects, etc., can generally be regarded as stationary in increments.

When the cross-variogram between two functions is zero, the functions are said to be fully spatially independent. In this case, it follows that the covariance and variogram functions induced by the sum $f + g$ are simply the sum of the respective covariance and variogram functions. That is, for f and g spatially independent

$$\mathrm{Cov}_{f+g}(h) = \mathrm{Cov}_f(h) + \mathrm{Cov}_g(h). \quad (8)$$

This notion can be used to construct models for covariances as the sum of spatially independent structures or as the result of linear combinations of spatially independent random functions. It will be seen, however, that most of

the more realistic models for images cannot be easily interpreted as the sum of spatially independent structures.

III. Covariance and Overlap Between Sets

A. Covariance for Random Sets

Thus far, our treatment has dealt with definitions of means, covariances, and variograms for random spatial functions. We now turn to consider these concepts as applied within and between spatial subsets of $\boldsymbol{R}^N$. This is important for two reasons. First, in the discrete-element scene model, objects have associated sizes and shapes. Since we will assume that the objects and background are internally homogeneous, the numerical difference between two points will be zero when they both fall within objects with the same spectral values, and some larger fixed values when they fall on object and background. Mathematically, this may be treated by defining a random family of subsets of $\boldsymbol{R}^N$ with size and shape properties characteristic of the object and examining the covariance structure that exists for the field containing the subset.

A second reason for examining the properties of spatial subsets is to understand the effects of regularization. In a digital image, the brightness value associated with a pixel is an integration of radiance over the spatial response function, or point spread function (PSF), of the instrument. The spatial area bounded by the line marking where the PSF falls to half of its peak value is called the effective instantaneous field of view (EIFOV), or optical pixel, for the instrument. The EIFOV is clearly a subset of $\boldsymbol{R}^2$. At this point, we will regard the instrument as having perfect response in that radiance is integrated equally over the EIFOV and no radiance enters from outside. That is, the EIFOV is the IFOV.

In mathematical terms, we can regard the IFOV or a discrete object as a random set ($\boldsymbol{X}$) within a two-dimensional field (Fig. 1(a)). Consider a point x within some space $\boldsymbol{T}$ of $\boldsymbol{R}^N$. Associated with any realization of the random set ($\boldsymbol{X}$) is an indicator function $I_{\boldsymbol{X}}(x)$

$$I_{\boldsymbol{X}}(x) = \begin{cases} 1, & x \text{ is in } \boldsymbol{X} \\ 0, & \text{else.} \end{cases} \tag{9}$$

If we consider many random placements of the set $\boldsymbol{X}$ onto the field $\boldsymbol{T}$, we can define $m(x)$ as

$$m(x) = \text{Prob}\{x \in \boldsymbol{X}\} = E\{I_{\boldsymbol{X}}(x)\} \tag{10}$$

where $\{x \in \boldsymbol{X}\}$ denotes the event that the realization of $\boldsymbol{X}$ contains the point x. If all placements are equally likely, $m(x)$ will be uniform over $\boldsymbol{T}$ and it will suffice to use $\boldsymbol{m}$ alone to refer to this probability.

To develop the concept of spatial covariance for the random set $\boldsymbol{X}$, consider another point $x + h$ located h away from x (Fig. 1(a)). We will define the covariance of the random set $\boldsymbol{X}$ as the covariance of the indicator functions for x and $x + h$. Substituting in (3)

$$\begin{aligned} \text{Cov}_{\boldsymbol{X}}(h) &= E\{[I_{\boldsymbol{X}}(x) - m][I_{\boldsymbol{X}}(x+h) - m]\} \\ &= E\{I_{\boldsymbol{X}}(x)\, I_{\boldsymbol{X}}(x+h)\} - m^2. \end{aligned} \tag{11}$$

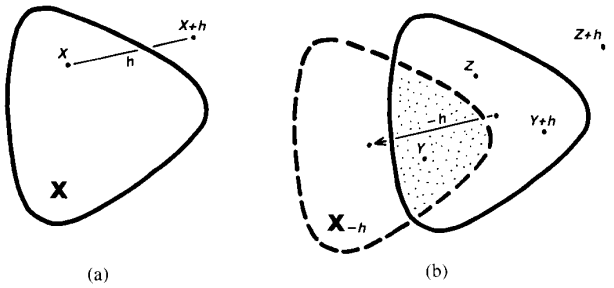

(a) (b)

Fig. 1. Diagrams of simple sets. (a) Points X and $X + h$ within region $\boldsymbol{X}$. (b) Illustration of $\boldsymbol{X} \cap \boldsymbol{X}_{-h}$ (stippled area). If a point falls within the stippled area (e.g., Y), then it will fall within $\boldsymbol{X}$ after a translation by distance h. If a point falls outside the stippled area (e.g., Z), then it will fall outside of $\boldsymbol{X}$ after translation by h.

Let us explore this further in the case where $\boldsymbol{X}$ is an object of fixed size and a realization is a random placement of $\boldsymbol{X}$. If h is larger than the width of $\boldsymbol{X}$, then the probabilities that $\boldsymbol{X}$ encloses x and that $\boldsymbol{X}$ encloses $x + h$ will be independent. Thus, the expectation of the product will be the product of the expectations, and

$$\begin{aligned} \text{Cov}_{\boldsymbol{X}}(h) &= E\{I_{\boldsymbol{X}}(x)\}\, E\{I_{\boldsymbol{X}}(x+h)\} - m^2 \\ &= m \cdot m - m^2 = 0. \end{aligned} \tag{12}$$

If $h = 0$, then x and $x + h$ coincide, and $E\{I_{\boldsymbol{X}}(x)\, I_{\boldsymbol{X}}(x + 0)\} = E\{[I_{\boldsymbol{X}}(x)]^2\}$. However, $I_{\boldsymbol{X}}(x)$ is an indicator function with values 1 or 0. Thus, $I_{\boldsymbol{X}}(x)^2 = I_{\boldsymbol{X}}(x)$, so

$$\begin{aligned} E\{I_{\boldsymbol{X}}(x)\, I_{\boldsymbol{X}}(x+0)\} &= m \\ \text{Cov}_{\boldsymbol{X}}(0) &= m - m^2 = m(1-m). \end{aligned} \tag{13}$$

Thus, $\text{Cov}_{\boldsymbol{X}}(h)$ will range between $m(1 - m)$ and 0.

The covariance can also be expressed in random set form, as

$$\begin{aligned} \text{Cov}_{\boldsymbol{X}}(h) &= \text{Prob}\{x \in \boldsymbol{X} \text{ and } x + h \in \boldsymbol{X}\} - m^2 \\ &= \text{Prob}\{x \in \boldsymbol{X} \cap \boldsymbol{X}_{-h}\} - m^2 \end{aligned} \tag{14}$$

where $\boldsymbol{X} \cap \boldsymbol{X}_{-h}$ denotes the intersection of $\boldsymbol{X}$ with $\boldsymbol{X}$ shifted by the increment $-h$. This form is illustrated in Fig. 1(b) where the stippled area corresponds to $\boldsymbol{X} \cap \boldsymbol{X}_{-h}$.

We may also define a variogram function for the random set $\boldsymbol{X}$ as

$$\begin{aligned} V_{\boldsymbol{X}}(h) &= E\{[I_{\boldsymbol{X}}(x) - I_{\boldsymbol{X}}(x+h)]^2\} \\ &= 2(\text{Cov}_{\boldsymbol{X}}(0) - \text{Cov}_{\boldsymbol{X}}(h)] \\ &= 2[m(1-m) - \text{Cov}_{\boldsymbol{X}}(h)] \\ &= 2m(1-m) - 2\,\text{Cov}_{\boldsymbol{X}}(h). \end{aligned} \tag{15}$$

In random set form

$$V_{\boldsymbol{X}}(h) = \text{Prob}\{x \in \boldsymbol{X} \cap \boldsymbol{X}^c_{-h}\} \tag{16}$$

where $\boldsymbol{X}^c_{-h}$ denotes the complement of $\boldsymbol{X}_{-h}$ (Fig. 2(a)).

B. Functional Covariances and Set Overlap Functions

In most cases, the images with which we work are, at best, a single realization of the random process consid-

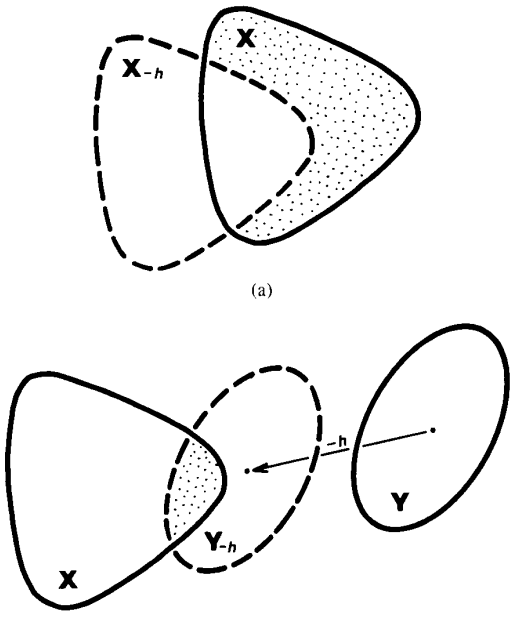

Fig. 2. More set diagrams. (a) $X \cap X^c_{-h}$ (stippled area) for set X translated $-h$. (b) $X \cap Y_{-h}$. $K_{XY}(h)$ is the overlap area indicated by the stipple.

ered thus far. The underlying discrete object scenes, for example, may be deterministic placements of objects that can only be modeled in this way as realizations of some random process. We must therefore relate the properties of the random regionalized variable to those of a realization of it.

If T is a subset of the space R^N and $f(x)$ is a function defined on T—which may be regarded either as a deterministic set function or as a realization of a random function

$$m = \int_T f(x)\, d|x| / \text{Mes}\,(T) \tag{17}$$

$$C_f(h) = \int_T f(x) f(x+h)\, d|x| / \text{Mes}\,(T) \tag{18}$$

$$V_f(h) = \int_T [f(x) - f(x+h)]^2\, d|x| / \text{Mes}\,(T) \tag{19}$$

may be defined and used as functions characterizing the function f within T. Mes (T) is the Lebesque measure of T, defined as

$$\text{Mes}\,(T) = \int_T d|x| = \int_{R^N} I_T(x)\, d|x| \tag{20}$$

where $I_T(x)$ is the indicator function for T. Mes (T), in the case of a two-dimensional image, thus corresponds to T's area. The notation $d|x|$ represents the infinitesimal volume element of integration $dx_1\, dx_2, \ldots, dx_n$.

The functions m and $C_f(h)$ can, as measures, be associated with a stochastic function for which they are the true mean and covariance [18], and under certain other assumptions, amounting to ergodicity of $f(x)$ [19], the spatial statistics for a single realization of $f(x)$ form unbiased estimates for the underlying covariance and mean.

For deterministic sets, the functions

$$\text{Mes}\,(X) = \int_X d|x| = \int_T I_X(x)\, d|x| \tag{21}$$

$$K_X(h) = \text{Mes}\,\{X \cap X_{-h}\} \tag{22}$$

$$V_X(h) = \text{Mes}\,\{X \cap X^c_{-h}\} \tag{23}$$

play similar roles to the spatial mean, autocovariance and variogram for deterministic functions. $K_X(h)$ is especially important in this work. However, it will not be called a covariance, but rather the set overlap function. In our two-dimensional example, these quantities correspond respectively to the area of X, the overlap of X with itself shifted by $-h$ (stippled portion of Fig. 1(b)), and the area of X not covered by X shifted $-h$ (stippled portion of Fig. 2(a)).

As with random functions, it is possible to define the equivalent of a cross-covariance for two deterministic sets X and Y as

$$K_{XY}(h) = \text{Mes}\,\{X \cap Y_{-h}\}. \tag{24}$$

This function measures the overlap between X and Y after shift $-h$ (Fig. 2(b)).

As with the spatial moments of functions, the (computable) overlap function provides an estimate for the covariance function induced by a random set function of which X is a realization. This estimate, however, only makes sense when the random set function has stationarity and ergodicity properties, which a single finite set does not have.

In general, when we have a finite realization of discrete sets in the plane as a scene model (such as agricultural fields or forest stands), the covariance is computed by assuming the sets to be observed in a bounded set T (the remotely sensed scene in our case) and using

$$\frac{\text{Mes}\,\{(X \cap T) \cap (X_{-h} \cap T)\}}{\text{Mes}\,(T)} - \left[\frac{\text{Mes}\,\{X \cap T\}}{\text{Mes}\,(T)}\right]^2 \tag{25}$$

as an estimate for the underlying covariance function

$$\text{Prob}\,\{x \in X \cap X_{-h}\} - m^2. \tag{26}$$

Unlike the covariance, the overlap function is defined for a single, finite set in the plane. In the papers following this one, we will use models in which the covariance of an image model may be defined in terms of the overlap functions of its discrete components. These "Boolean" models [15] will be based on definitions of this section.

C. Covariance Between Sets

If A and B are two fixed sets in R^N, the covariance between them, induced by $\text{Cov}_f(x_1, x_2)$ with x_1 contained

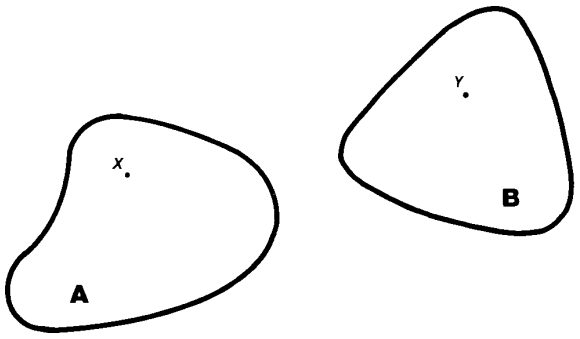

Fig. 3. Two random sets A and B containing points x and y.

in A and x_2 contained in B is

$$\mathrm{Cov}_f(A, B) = \int_{A\times B} \mathrm{Cov}_f(x_1, x_2)\, d|x_1| \cdot d|x_2| / \mathrm{Mes}(A)\ \mathrm{Mes}(B). \quad (27)$$

This situation is diagrammed in Fig. 3. $\mathrm{Cov}_f(A, B)$ can be thought of as the average covariance between all points x within A and y within B. When A and B are identical, then the result is the variance of the set A

$$\mathrm{Cov}_f(A, A) = \int_{A\times A} \mathrm{Cov}_f(x_1, x_2)\, d|x_1| \cdot d|x_2| / \mathrm{Mes}^2(A) = \sigma_A^2 \quad (28)$$

where x_1 and x_2 are two points within A.

If the underlying covariance is stationary (or rather depends only on increment h), it may be shown that

$$\mathrm{Cov}_f(A, B) = \int_{R^N} K_{AB}(h)\ \mathrm{Cov}_f(h) \cdot d|h| / \mathrm{Mes}(A)\ \mathrm{Mes}(B). \quad (29)$$

The covariance between the two sets thus depends on the product of two functions: the covariance function $\mathrm{Cov}_f(h)$, and the overlap function $K_{AB}(h)$. Their product will be positive only when $K_{AB}(h)$ is nonzero—i.e., when there is overlap between the two sets at distance h—and when there is a nonzero covariance at that distance. When A and B are the same set, it follows that

$$\mathrm{Cov}_f(A, A) = \sigma_A^2 = \int_{R^N} K_A(h) \cdot \mathrm{Cov}_f(h)\, d|h| / \mathrm{Mes}^2(A). \quad (30)$$

The covariance and overlap functions occurring in this integral are illustrated in Fig. 4.

Expression (29) is the fundamental relation between the set overlap function and a covariance between sets induced by a random function. It is at the base of much statistical estimation in geostatistics and has some interesting interpretations.

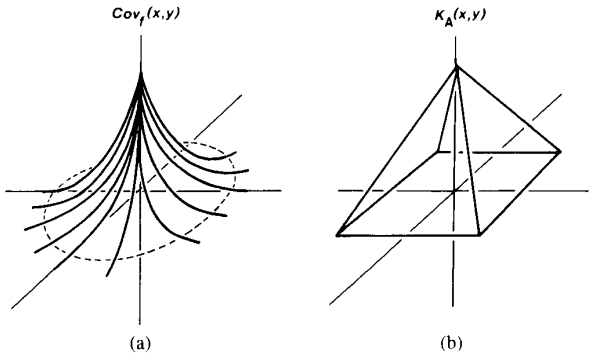

Fig. 4. Sketches of covariance and overlap functions in two dimensions. Axes are x and y coordinates resolved from h. The origin is $h = 0$. (a) Covariance function for a regionalized variable, modeled as a negative exponential function. Dashed line, contour at value near 0. Values are significantly greater than zero only within the contour. (b) Overlap function. A square-based pyramid is shown, which is appropriate for a square-shaped set overlapping (without rotation) with itself.

D. Normalized Overlap Functions

Let

$$H_{AB}(h) = K_{AB}(h)/\mathrm{Mes}(A)\ \mathrm{Mes}(B) \quad (31)$$

be a normalized overlap function for the deterministic sets A and B. It is, in fact, identical with the distribution function for the lengths of vectors h with end points in A and B, respectively [20]. The function $H_A(h)$, defined similarly using $K_A(h)$, is identical with the distribution function for the lengths of vectors with both ends in A. The normalized overlap functions $H_{AB}(h)$ and $H_A(h)$ have unit mass, and thus the fundamental relation between set covariance and covariance between sets (29) becomes

$$\mathrm{Cov}_f(A, B) = \int_{R^N} H_{AB}(h)\ \mathrm{Cov}_f(h)\, d|h| \quad (32)$$

$$\mathrm{Cov}_f(A, A) = \sigma_A^2 = \int_{R^N} H_A(h)\ \mathrm{Cov}_f(h)\, d|h|. \quad (33)$$

Hence, the set covariance or overlap function $H_{AB}(h)$ transforms the covariance function $\mathrm{Cov}_f(h)$ into an induced covariance between the sets.

The sets A and B are, at this point, arbitrary sets. They could, for example, be two management zones (e.g., states) from a map, so that $\mathrm{Cov}_f(A, B)$ would represent a covariance between the zones induced by a regionalized variable—such as population density. However, in the context of remote sensing and images, A and B are usually two instantaneous fields of view that are similar in size and shape but are shifted a distance h from one another. This situation leads to some especially useful forms of (32) and (33).

E. Convolution and Shifted Set Functions

The form of the deterministic (auto)covariance function

$$C_f(h) = \int_T f(x) f(x + h)\, d|x| / \mathrm{Mes}(T) \quad (34)$$

in the case where $f(x)$ and $f(x + h)$ vanish outside $\boldsymbol{T}$ is that of a convolution integral between f and its conjugate $\bar{f}$ normalized by Mes ($\boldsymbol{T}$). Algebraically this can be written

$$C_f(h) = f * \bar{f}(h)/\text{Mes}\ (\boldsymbol{T}) \tag{35}$$

where the convolution operator $*$ is defined by

$$f * g(h) = \int_{\boldsymbol{R}^N} f(x)\, g(h - x)\, d|x| \tag{36}$$

and $\bar{f}(x) = f(-x)$ when f is real. The properties of convolution are well established in many texts [19], [21] and the Fourier domain properties are of special value for many problems.

For sets, if $I_A(x)$ is the indicator function for $\boldsymbol{A}$ and $I_B(x)$ is the indicator function for $\boldsymbol{B}$, then the function $H_{AB}(h)$ defined above may be written

$$\begin{aligned} H_{AB}(h) &= \int_{\boldsymbol{R}^N} I_A(x)\, I_B(x + h)\, d|x|/\text{Mes}\ (\boldsymbol{A})\ \text{Mes}\ (\boldsymbol{B}) \\ &= I_A * \bar{I}_B(h)/\text{Mes}\ (\boldsymbol{A})\ \text{Mes}\ (\boldsymbol{B}) \\ &= \text{Mes}\ (\boldsymbol{A} \cap \boldsymbol{B}_{-h})/\text{Mes}\ (\boldsymbol{A})\ \text{Mes}\ (\boldsymbol{B}). \end{aligned} \tag{37}$$

Now consider the case in which $\boldsymbol{A}$ and $\boldsymbol{B}$ are the same set $\boldsymbol{Z}$, but are translated by distance p. This case includes the situation in which $\boldsymbol{Z}$ is the IFOV of a remote-sensing instrument and $\boldsymbol{A}$ and $\boldsymbol{B}$ are thus two successive fields of view separated by a distance p. In this case it is possible to show for a translation of $-p$ that

$$\begin{aligned} H_{\boldsymbol{Z}\boldsymbol{Z}_{-p}}(h) &= \text{Mes}\ (\boldsymbol{Z} \cap \boldsymbol{Z}_{-(h+p)})/\text{Mes}^2\ (\boldsymbol{Z}) \\ &= H_{\boldsymbol{Z}\boldsymbol{Z}_{-h}}(p) = H_{\boldsymbol{Z}}(p + h) \end{aligned} \tag{38}$$

or, in convolution notation

$$I_{\boldsymbol{Z}} * \bar{I}_{\boldsymbol{Z}_{-p}}(h) = I_{\boldsymbol{Z}} * \bar{I}_{\boldsymbol{Z}}(p + h). \tag{39}$$

It follows from (32) that

$$\begin{aligned} \text{Cov}_f(\boldsymbol{Z}, \boldsymbol{Z}_{-p}) &= \int_{\boldsymbol{R}^N} H_{\boldsymbol{Z}}(p + h)\, \text{Cov}_f(h)\, d|h| \\ &= H_{\boldsymbol{Z}} * \text{Cov}_f(p). \end{aligned} \tag{40}$$

And, substituting from (39)

$$\text{Cov}_f(\boldsymbol{Z}, \boldsymbol{Z}_{-p}) = (I_{\boldsymbol{Z}} * \bar{I}_{\boldsymbol{Z}}) * \text{Cov}_f(p)/\text{Mes}^2\ (\boldsymbol{Z}). \tag{41}$$

As before, a variogram function between sets can be defined and in this case we have

$$\begin{aligned} V_f(\boldsymbol{Z}, \boldsymbol{Z}_{-p}) &= \text{Cov}_f(\boldsymbol{Z}, \boldsymbol{Z}) - \text{Cov}_f(\boldsymbol{Z}, \boldsymbol{Z}_{-p}) \\ &= \sigma_{\boldsymbol{Z}}^2 - \text{Cov}_f(\boldsymbol{Z}, \boldsymbol{Z}_{-p}) \\ &= \sigma_{\boldsymbol{Z}}^2 - H_{\boldsymbol{Z}} * \text{Cov}_f(p). \end{aligned} \tag{42}$$

Equation (40) may be developed further when the model is defined in the plane ($\boldsymbol{R}^2$) and the covariance is isotropic (that is, depends only on $r = |h|$). Then, by changing variables to polar coordinates ($x = r \sin\theta$, $r \cos\theta$), it follows that

$$\text{Cov}_f(\boldsymbol{Z}, \boldsymbol{Z}_{-p}) = C_{\boldsymbol{Z}}(p) = \int_0^\infty r\boldsymbol{T}_{\boldsymbol{Z}}(p, r)\, C(r)\, dr \tag{43}$$

where

$$\boldsymbol{T}_{\boldsymbol{Z}}(p, r) = \int_{-\pi}^{\pi} H_{\boldsymbol{Z}}(x + p)\, d\theta \tag{44}$$

and $H_{\boldsymbol{Z}}$ is the overlap function for $\boldsymbol{Z}$ normalized so that as $|\boldsymbol{Z}| \to 0$, $C_{\boldsymbol{Z}}(p) \to C(p)$. That is

$$\int_0^\infty r \int_{-\pi}^{\pi} H_{\boldsymbol{Z}}(x)\, d\theta\, dr = 1. \tag{45}$$

This form for the covariance allows a particularly convenient form for the regularized variance to be developed for isotropic covariances. That is

$$\begin{aligned} \sigma_{\boldsymbol{Z}}^2 &= \int_0^\infty r\boldsymbol{T}_{\boldsymbol{Z}}(0, r)\, C(r)\, dr \\ &= \int_0^\infty \phi(r)\, C(r)\, dr. \end{aligned} \tag{46}$$

In this case, $\phi(r)$ is the distribution function for lengths r in $\boldsymbol{Z}$ and may be explicitly computed for a variety of shapes for $\boldsymbol{Z}$, as shown by Garwood [22]. The covariance, however, is quite complicated and must usually be computed numerically—and is often better computed using (40), even for isotropic underlying covariances.

IV. Regularization of Scenes and Examples of Simple Covariance Functions

A. Regularization of Scenes

Equation (41) provides the basis for understanding the effects of regularization on the covariance structure of an image, and is known as Matheron's Theorem [12]. From the equation, two functions are involved. One of these is the underlying covariance function Cov_f, which is taken to be an intrinsic property of the scene. The second is a function derived from the area over which regularization occurs—in this case, $I_{\boldsymbol{Z}} * \bar{I}_{\boldsymbol{Z}_{-p}}(h)$ or $H_{\boldsymbol{Z}}(h)$, where the convolution describes the overlap of the regularizing area with itself at distance h. The theorem then states that the covariance induced by f between a set $\boldsymbol{Z}$ and the same set translated a distance p is the value at step p of the convolution between the underlying covariance induced by f and the normalized set overlap function associated with $\boldsymbol{Z}$—that is, $H_{\boldsymbol{Z}}(h)$.

The immediate application of this to remote sensing occurs when the scene is modeled as a realization of a regionalized variable and the image is taken to be a regular set of samples from the scene integrated over pixels that are shifts of a basic IFOV (Fig. 5). In this case, the measurable statistic, i.e., covariance between pixels over the extent of the image (which is taken to be the set $\boldsymbol{T}$), is an estimate for the regularized covariance. This is related

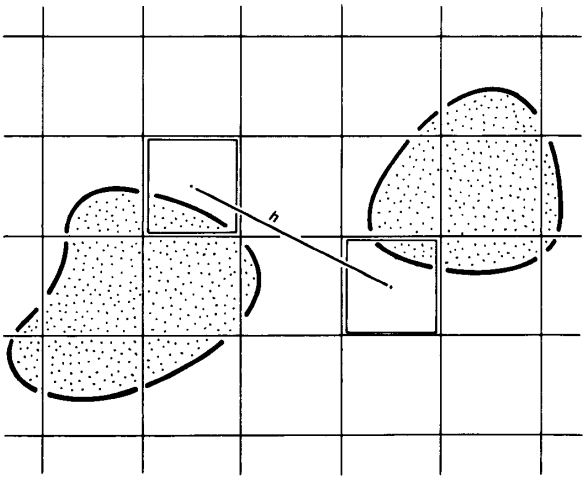

Fig. 5. Discrete-element scene as imaged by pixels that are integral shifts of a square IFOV.

directly with the underlying covariance $H_Z(h)$ and Matheron's Theorem.

It is useful, at this point, to examine some simple overlap functions (H_Z) of this nature. The one-dimensional case is perhaps the simplest. Consider an indicator function

$$I_X(x) = \begin{cases} 1, & \text{if } -a \le x \le a \\ 0, & \text{else.} \end{cases} \tag{47}$$

The overlap function associated with the interval a for a distance h will be

$$K_a(h) = I_X * \bar{I}_X(h) = \int I_X(x)\, I_X(x+h)\, d|x| = \begin{cases} 2a - |t|, & |t| \le a \\ 0, & |t| > a \end{cases} \tag{48}$$

This function is illustrated in Fig. 6. $I_X(x)$ is a "boxcar" centered on $x = 0$, $I_X(x+h)$ is a similar boxcar centered on $-h$, and $I_X * \bar{I}_X(h)$ is the integral of the indicator function in the area of intersection between the two. The resulting $K_a(h)$ is a triangle with base $4a$ and height $2a$.

A two-dimensional situation may be more relevant to image models. Consider a circular regularizing area of radius a with an indicator function

$$I_X(x) = \begin{cases} 1, & \text{if } |x| \le a \\ 0, & \text{else.} \end{cases} \tag{49}$$

This function has the shape of a discoid (Fig. 7). The convolution of the indicator function is the volume of overlap between the discoid centered at $x = y = 0$ and at $-h$. Some simple geometry shows this function to be

$$K_a(|h|) = \frac{A}{\pi}(\theta - \sin\theta) \tag{50}$$

where A is the area of the regularizing disk ($= \pi a^2$) and $\cos(\theta/2) = |h|/(2a)$.

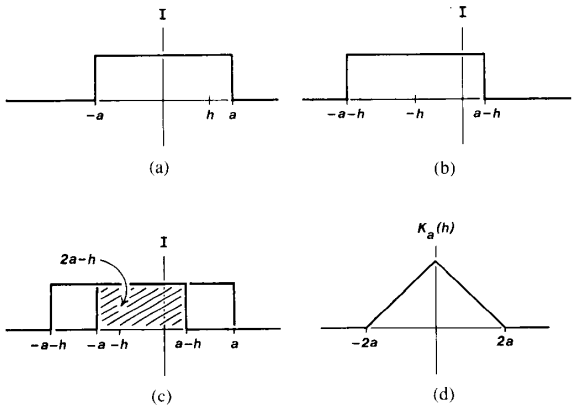

Fig. 6. Convolution of indicator function, one-dimensional example. (a) Indicator function for length a. The function has height unity. (b) Indicator function shifted $-h$. (c) Overlap of function with itself shifted $-h$. Convolution $I_x * \bar{I}_x(h)$, which has area $2a - h$, is hatched. (d) Overlap function $K_a(h)$, which has maximum value $2a$.

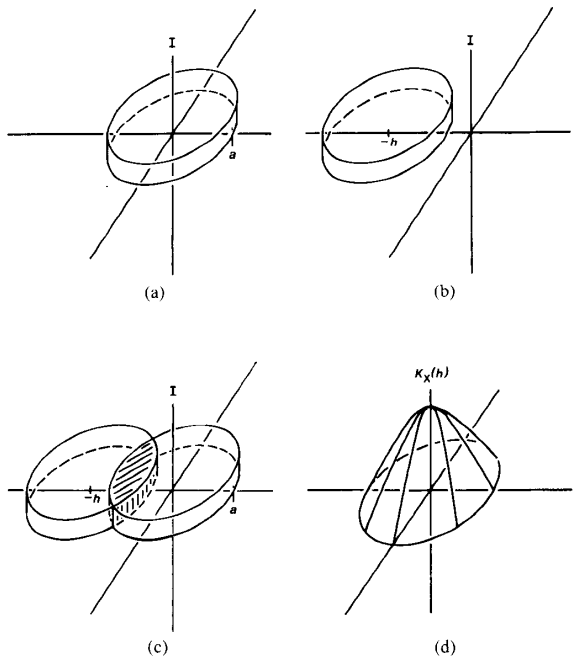

Fig. 7. Illustration of overlap function for a disk. (a) Indicator function drawn as a discoid. Height of discoid is unity. (b) Indicator function shifted by $-h$. (c) Overlap of function with itself shifted $-h$. Convolution $I_X * \bar{I}_X(h)$ is shown by hatching. (d) Overlap function $K_X(h)$.

A zero-one indicator function implies in a remote-sensing situation that the sensing device has a square-wave response function, integrating all energy equally within the IFOV and rejecting all energy outside of it. In the case of a real sensor, this is probably an unrealistic assumption. Suffice it to say, however, that, given a real modulation transfer function, it is a straightforward modification to derive, at least numerically, a solution for the overlap function.

B. One-Dimensional Exponential Case

In one dimension, regularization occurs when an underlying random function is known, or measured, by integration over finite intervals. Data loggers, or integrating instruments such as rain gauges, provide examples where time series of somewhat random events are integrated (regularized) and where the relationship between the underlying covariance and the covariance between the integrated measurements is of great importance.

A common form of covariance function for time series of this kind is the exponential covariance

$$C(h) = \sigma^2 e^{-\alpha|h|} \tag{51}$$

where α describes the dependence of covariance on distance. The data, however, only give estimates for the integrated data and therefore the regularized covariance

$$C_a(h) = \frac{\sigma^2}{2a^2} \int_{-\infty}^{\infty} K_a(h + r)\, e^{-\alpha|r|}\, dr \tag{52}$$

where $K_a(h)$ is the function shown in Fig. 6(d). This integral is computable, leading to expressions for the regularized variogram and total variance of the form

$$V_a(h) = \sigma_a^2 - \frac{\sigma^2}{(2\alpha a)^2}(1 - e^{-2\alpha a})(e^{2\alpha a} - 1)e^{-\alpha|h|} \tag{53}$$

where

$$\sigma_a^2 = \frac{\sigma^2}{\alpha a}\left[1 - \frac{1}{2\alpha a}(1 - e^{-2\alpha a})\right] \tag{54}$$

when $h > 2a$, which is the practical case. Significantly, for $h > 2a$, $V_a(h)$ has the form of an exponential with the same exponent so that even with regularizing, the form of the covariance and variogram is still an exponential of the same general type.

Fig. 8 shows the behavior of $V_a(h)$ as a function of the integration interval (a). As the integration increases, the global variance σ_a^2 decreases and the variogram increases more slowly to its final level. The graphs are stepped to show the practical effect of regularization on data availability. Fig. 9 presents a plot of log σ_a^2 against log a. For small a, σ_a^2 is near σ^2 and falls slowly, showing spatial correlation. As a becomes large, the variance reduces as $1/a$, as would be expected of an uncorrelated random function, which in this case means that the structure is lost.

The significance of these plots is that all of the variation they illustrate has been created by the effects of regularization, or, for remotely sensed data, by the integration of the scene radiance with the underlying exponential covariance into pixels with a finite IFOV.

C. Two-Dimensional Exponential Case

In two dimensions, the exponential covariance is again a common model for two-dimensional spatially correlated fields. Here, regularizing corresponds to integration over an area such as a disk (Fig. 7) or a square (Fig. 4) and using (43). In this case, even for simple isotropic models like the exponential, the integral needs to be evaluated numerically.

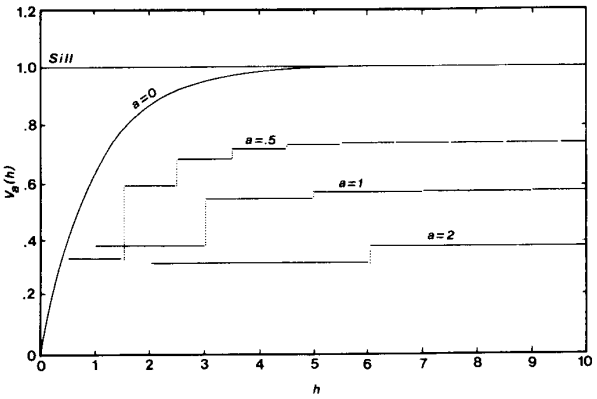

Fig. 8. Variogram for the one-dimensional exponential model as regularized for various intervals a. ($a = 0$, unregularized variogram; σ^2, $\alpha = 1$.)

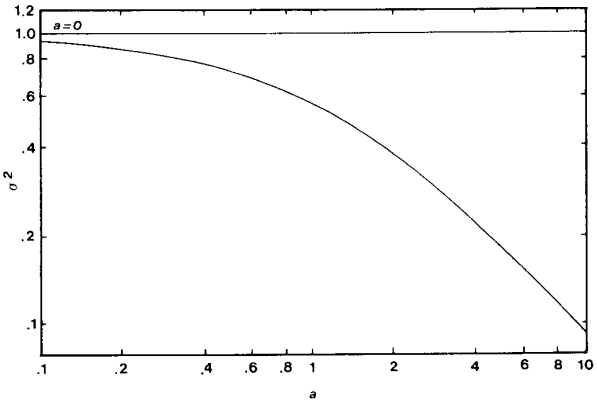

Fig. 9. Log-log relationship between σ_a^2, the regularized variance, and a, the regularizing interval, for the one-dimensional exponential model. Horizontal line—unregularized variance ($a = 0$). (σ^2, $\alpha = 1$.)

For the simple exponential covariance $C(h) = e^{-h}$ and variogram $V(h) = 1 - e^{-h}$, we have plotted graphs in Fig. 10 showing $V_a(h)$ as a function of a, where a is now the radius of the regularizing disk. Similarly, in Fig. 11 we have plotted log σ_a against log a which again shows how for large a the behavior of the variance is similar to that of an uncorrelated random function. However, for small a, the behavior is not.

Again, the plots show how the effect of averaging over the IFOV in remotely sensed data will introduce significant changes in the covariance derived from the data relative to the underlying covariance. A comparison between Figs. 8 and 9, and Figs. 10 and 11, also shows how dimensionality is significant as well. Integration along lines behaves differently from integration over a disk, even for isotropic covariances. Geometric effects will become even more significant when the data involve an oblique (projective) IFOV of a three-dimensional scene.

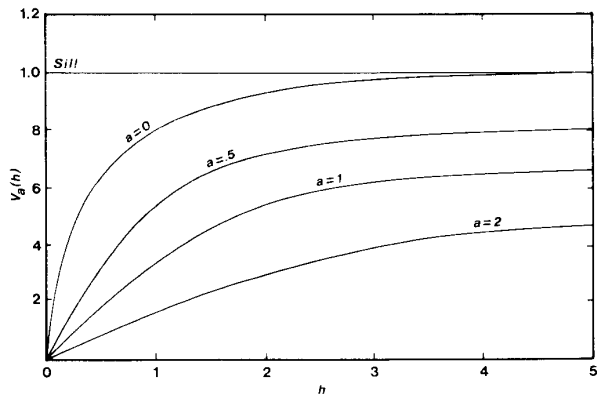

Fig. 10. Variograms for the two-dimensional exponential model with varying degrees of regularization by a disc of radius a. ($a = 0$, unregularized variogram; σ^2, $\alpha = 1$.)

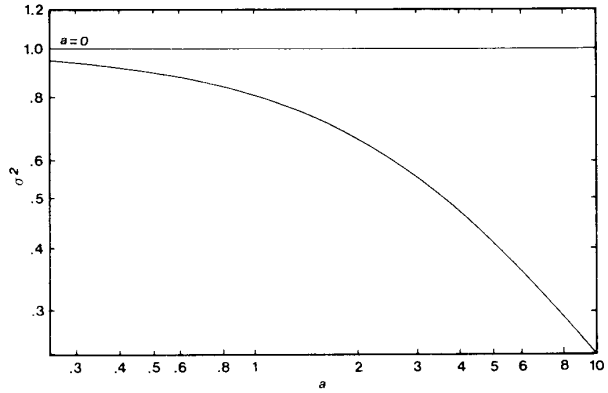

Fig. 11. Log-log relationship between regularized variance σ_a^2, and the radius a of the regularizing disk for the two-dimensional exponential model. Horizontal line—unregularized variance ($a = 0$). (σ^2, $\alpha = 1$.)

D. Other Models

Similar plots and studies on their properties may be derived for a variety of isotropic covariance functions. Three of these are worth presenting briefly. First is the Bessel covariance [23]

$$C(h) = \sigma^2 h K_1(ah) \tag{55}$$

which provides a natural generalization of the exponential covariance to two dimensions. Another is the well known "spherical" covariance [15]

$$C(h) = \begin{cases} \sigma^2\left[1 - \frac{3}{2}\frac{|h|}{D} + \left(\frac{|h|}{D}\right)^3\right], & |h| < D \\ 0, & |h| > D \end{cases}$$

which is the overlap function for a sphere of diameter D and has been used as a model for both one- and two-dimensional covariances in geostatistics. Last is the "independent structures" model (see Section II-C) consisting of a linear combination of N exponential models

$$C(h) = \sigma^2 \sum_{i=1}^{N} \omega_i e^{-a_i} \tag{56}$$

where each $\omega_i > 0$, $\Sigma\, \omega_i = 1$, and $a_i > 0$ for $i = 1$ to N. In this model, independent regionalized variables with short "range" and long "range" can be combined to model almost any observed covariance [24].

At this stage, it is clear that the functional relationships between the parameters of an underlying covariance and the (observed) regularized estimate of the covariance may be computed explicitly. The examples given above, however, were mathematical and not derived from a model (in the case of remote sensing) for the scene being imaged. For a class of scene models, it is possible to use the methods developed here to derive the scene covariance and the effects of regularization as a function of the parameters (e.g., size and spacing of discrete objects) describing the scene. When this occurs, (41) forms the basis for the inference of parameters of the scene models. The development of such scene models is the basis for Part II of this series of papers.

V. Conclusion

In this paper (Part I), we have examined how the covariance and variogram, which describe the spatial structure of a scene, are modified when the scene is imaged by integration into pixels with finite EIFOV. We have also established a framework for estimating covariances of set functions and between sets. This framework was used here for modeling the effect of pixel size on the underlying covariance but can also be used to model the underlying covariance of scenes composed of discrete objects.

Together, these results allow us to develop a theory of scene parameter inference from remotely sensed data. Firstly, relationships must be established between the scene parameters and the underlying covariance structure. Secondly, the effect of the infinite IFOV must be established. There follows a complete model for the relationship between scene parameters and image data, which will be further investigated for simple scene models in Part II of this paper.

References

[1] X. Li and A. H. Strahler, "Geometric-optical modeling of a conifer forest canopy," *IEEE Trans. Geosci. Remote Sensing*, vol. GE-23, pp. 705–721, 1985.

[2] ——, "Geometric-optical bidirectional reflectance modeling of a conifer forest canopy," *IEEE Trans. Geosci. Remote Sensing*, vol. GE-24, pp. 906–919, 1986.

[3] C. E. Woodcock, "Understanding spatial variation in remotely sensed imagery," Ph.D. dissertation, Univ. California, Santa Barbara, 1985.

[4] C. E. Woodcock and A. H. Strahler, "The factor of scale in remote sensing," *Remote Sensing Environ.*, vol. 21, pp. 311–322, 1987.

[5] C. E. Woodcock, A. H. Strahler, and D. L. B. Jupp, "The use of variograms in remote sensing I: Scene models and simulated images," *Remote Sensing Environ.*, in press, 1988.

[6] ——, "The use of variograms in remote sensing II: Real digital images," *Remote Sensing Environ.*, in press, 1988.

[7] J. Walker, D. L. B. Jupp, L. K. Penridge, and G. Tian, "Interpretation of vegetation structure in Landsat MSS imagery: A case study in disturbed semi-arid eucalypt woodlands. Part I. Field data analysis," *J. Environ. Management*, vol. 23, pp. 19–33, 1986.
[8] D. L. B. Jupp, J. Walker, and L. K. Penridge, "Interpretation of vegetation structure in Landsat MSS imagery: A case study in disturbed semi-arid eucalypt woodlands. Part 2. Model-based analysis," *J. Environ. Management*, vol. 23, pp. 35–57, 1986.
[9] A. H. Strahler, X. Li, C. E. Woodcock, and D. L. B. Jupp, "Discrete-object modeling of remotely sensed scenes," in *Proc. 19th Int. Symp. Remote Sensing Environ.* (Paris, France), pp. 465–473, 1985.
[10] A. H. Strahler, C. E. Woodcock, and J. A. Smith, "On the nature of models in remote sensing," *Remote Sensing Environ.*, vol. 20, pp. 121–139, 1986.
[11] C. J. Huijbregts, "Regionalized variables and quantitative analysis of spatial data," in *Display and Analysis of Spatial Data*, J. C. Davis and M. J. McCullagh, Eds. London: Wiley, 1975, pp. 38–53.
[12] G. Matheron, "Principles of geostatistics," *Economic Geology*, vol. 58, pp. 1246–1266, 1963.
[13] ——, *Les Variables Regionalisées et Leur Estimation*. Paris: Masson et Cie., 1965.
[14] ——, "The theory of regionalized variables and its applications," *Cahiers du Centre de Morphologie Mathematique de Fontainebleau*, no. 5, 1971.
[15] J. Serra, *Image Analysis and Mathematical Morphology*. London: Academic, 1982.
[16] L. S. Gandin, *Objective Analysis of Meteorological Fields*. Transl. from Russian by Israel Program for Scientific Translations, Springfield, VA, 1963.
[17] G. H. Jowett, "Sampling properties of local statistics in stationary stochastic series," *Biometrika*, vol. 42, pp. 160–169, 1955.
[18] J. L. Doob, *Stochastic Processes*. New York: Wiley, 1953.
[19] H. Cramer and M. R. Ledbetter, *Stationary and Related Stochastic Processes*. New York: Wiley, 1967.
[20] B. Matern, "Spatial variation: Stochastic models and their application to some problems in forest surveys and other sampling investigations," *Meddelanden Fran Statens Skogsforskningsinstitut*, band 49, nr. 5, pp. 1–144, 1960.
[21] A. M. Yaglom, *An Introduction to the Theory of Stationary Random Functions*. Englewood Cliffs, NJ: Prentice-Hall, 1962.
[22] F. Garwood, "The variance of the overlap of geometrical figures with reference to a bombing problem," *Biometrika*, vol. 34, pp. 1–17, 1947.
[23] P. Whittle, "On the variation of yield variance with plot size," *Biometrika*, vol. 43, pp. 336–342, 1956.
[24] N. Cressie, "Fitting variogram models by weighted least squares," *Math. Geology*, vol. 17, pp. 563–586, 1985.

David L. B. Jupp received the B.Sc.(Hon) degree from Adelaide University and the Ph.D. degree from Flinders University (both in South Australia) in 1969 and 1973, respectively, majoring in applied mathematics.

He has worked in areas of geophysical inversion and remote sensing. He is currently a Principal Research Scientist with the CSIRO Division of Water Resources in Canberra, Australia. His work there involves remote-sensing applications in the water industry, commercial image processing systems development and research into model-based interpretation of image data.

*

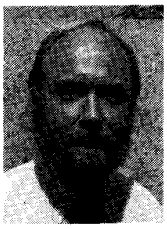

Alan H. Strahler received the B.A. and Ph.D. degrees from the Johns Hopkins University in 1964 and 1969, respectively.

He is currently Professor and Chair of the Department of Geology and Geography at Hunter College of the City University of New York. He has held prior academic positions at the University of California, Santa Barbara, and at the University of Virginia. Originally trained as a biogeographer, he has been actively involved in remote-sensing research since 1978. He has been a Principal Investigator on numerous NASA contracts and grants. His primary research interests are in spatial modeling and spatial statistics as they apply to remote sensing, and in geometric-optical modeling of remotely sensed scenes.

*

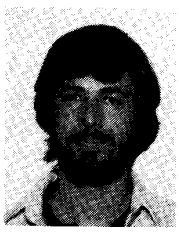

Curtis E. Woodcock received the B.A., M.A., and Ph.D. degrees from the Department of Geography, University of California, Santa Barbara.

He is currently an Assistant Professor in the Department of Geography and Acting Director of the Center for Remote Sensing at Boston University. Applications of remote sensing to forest inventory and other problems in natural environments have been a primary research interest. He has conducted both empirical and theoretical studies on the spatial properties of images, assessing the influence of both spatial resolution and the nature of environments on observed spatial patterns. The ability to incorporate other types of data in remote sensing analyses, such as digital elevation models, has resulted in an interest in geographic information systems.

Dr. Woodcock is a member of the American Society of Photogrammetry and Remote Sensing.